Fibroblast activation protein regulates natural killer cell migration, extravasation and tumor infiltration

Authors: Allison A. Fitzgerald[1], Emily F. Marcisak[2,3], Apsra Nasir[1], Eric Glasgow[1], Sandra A. Jablonski[1], Pieter Van Der Veken[4], Gray Pearson[1], Elana J. Fertig[3,5,6], Emily M. Mace[7], Louis M. Weiner[1*]

Affiliations:

[1]Department of Oncology, Georgetown Lombardi Comprehensive Cancer Center, Georgetown University Medical Center, Washington, DC, USA.

[2]McKusick-Nathans Institute of the Department of Genetic Medicine, Johns Hopkins School of Medicine, Baltimore, MD, USA.

[3]Department of Oncology, Sidney Kimmel Comprehensive Cancer Center, Johns Hopkins School of Medicine, Baltimore, MD, USA.

[4]Department of Medicinal Chemistry/UAMC, University of Antwerp, Universiteitsplein 1, B-2610 Wilrijk, Belgium.

[5]Department of Applied Mathematics and Statistics, Johns Hopkins University Whiting School of Engineering, Baltimore, MD, USA.

[6]Department of Biomedical Engineering, Johns Hopkins University School of Medicine, Baltimore, MD, USA.

[7]Department of Pediatrics, Columbia University Irving Medical Center, New York, NY, USA.

[*]Corresponding author email: weinerl@georgetown.edu

Abstract:

Natural killer (NK) cells play critical roles in physiologic and pathologic conditions such as pregnancy, infection, autoimmune disease and cancer. In cancer, numerous strategies have been designed to exploit the cytolytic properties of NK cells, with variable success. A major hurdle to NK-cell focused therapies is NK cell recruitment to and infiltration into tumors. While the chemotaxis pathways regulating NK recruitment to different tissues are well delineated, the mechanisms human NK cells employ to physically migrate are ill-defined. We show for the first time that human NK cells express fibroblast activation protein (FAP), a cell surface protease previously thought to be primarily expressed by activated fibroblasts. FAP degrades the extracellular matrix to facilitate cell migration and tissue remodeling. We used novel *in vivo* zebrafish and *in vitro* 3D culture models to demonstrate that FAP regulates NK cell migration, extravasation, and infiltration into tumors, ultimately affecting tumor cell lysis. These findings demonstrate the necessity of proteolytic migration in NK cell function, suggest novel mechanisms of action of FAP targeting drugs, and provide an entirely new way to regulate NK cell activity.

Graphical Abstract

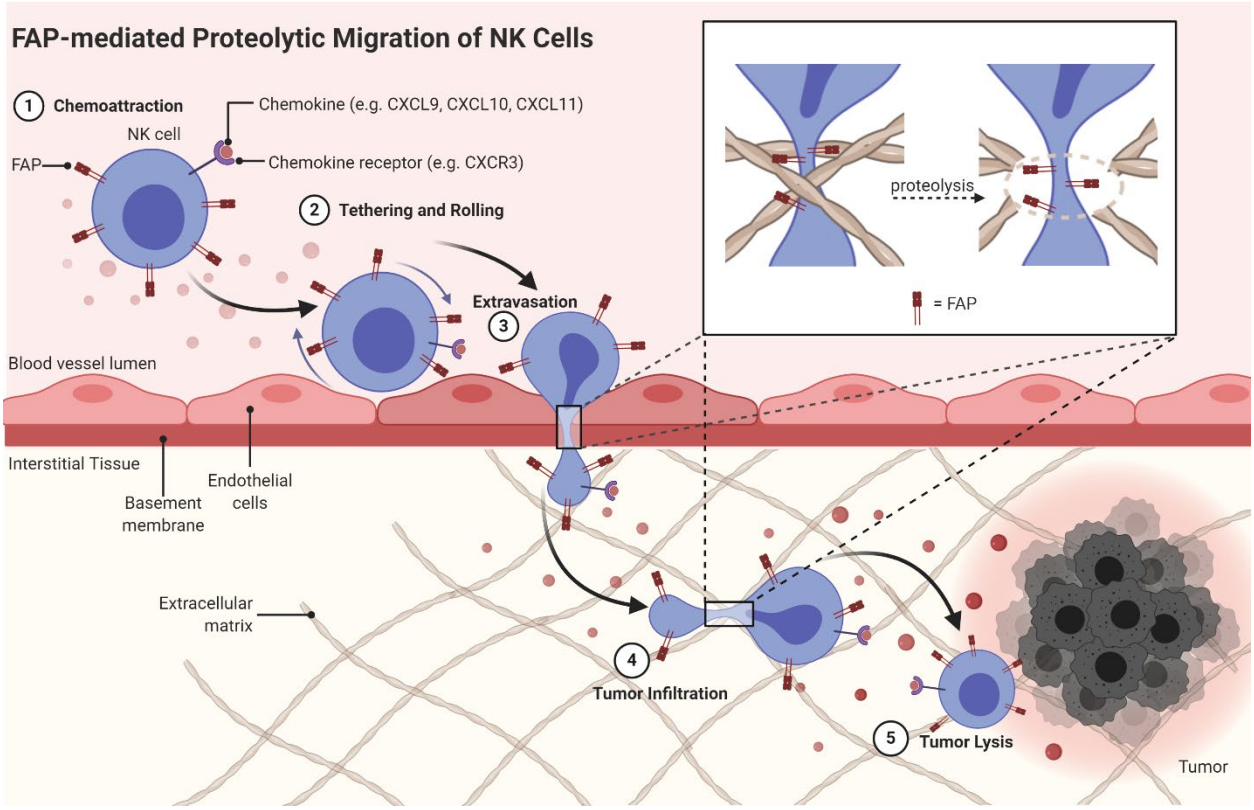

Introduction

Natural killer (NK) cells are innate lymphoid cells that influence many physiologic and pathologic conditions—especially viral infections and cancers—through their effector and regulatory cell functions (*1*). NK cells are canonically known to recognize and kill aberrant cells, such as virus-infected or malignant cells, using a complex detection system comprised of multiple inhibitory and activating receptors. Beyond their roles as effector cells, NK cells also regulate the functions of other cells types, such as dendritic cells, T cells, B cells and endothelial cells, through the release of immunomodulating cytokines (*2–6*). Because of their central role in the immune system and disease etiologies, efforts to manipulate NK cell activity have long been sought and developed to improve patient outcomes across many medical fields.

In cancer, patients with high tumoral NK cell content and activation have improved survival (*7*, *8*) and response to immunotherapy (*9–11*). Thus, NK cells are emerging as major targets to promote cancer immunotherapy (*12*). Current NK-focused immunotherapy approaches include autologous or allogenic NK cell transfer (*13*), CAR NK cells (*14*), NK immune checkpoint inhibitors (*15*), bi- or tri-specific killer engagers (BiKEs and TriKES) (*16*), and cytokine super-agonists (*17*). An impediment to all these therapies is inadequate NK cell homing to and/or infiltration into solid tumors.

Strategies that increase NK cell infiltration into tumors represent plausible ways to enhance NK cell-related antitumor immunotherapies. Such work has focused almost entirely on modulating NK chemokine receptors and chemoattractants (*18*, *19*) . However, lymphocyte migration depends on more than just chemotaxis. For NK cells to successfully infiltrate any tissue, including solid tumors, they must traverse complex microenvironments (e.g., extravasation from blood vessels and navigation through dense extracellular matrices) (*20*).

Beyond the chemokine/chemoattractant system, little is known about the mechanisms NK cells employ to physically migrate through these tissues.

Here we describe for the first time that human NK cells express fibroblast activation protein (FAP). FAP is a transmembrane serine protease primarily expressed on activated fibroblasts during wound healing or pathological conditions such as fibrosis, arthritis, and cancer (*21*). Since FAP is overexpressed in diseased tissue yet mostly absent from healthy tissue (*21*), it is a promising therapeutic target in conditions like cardiac fibrosis (*22*) and cancer (*23*). FAP is primarily known for its extracellular matrix remodeling capabilities due to its collagenase activity.

After identifying FAP expression by human NK cells, we used computational approaches to elucidate FAP's function in NK cells. We validated these computational findings using 2D assays. We then explored the impact of FAP inhibition on NK cell migratory properties such as extravasation using zebrafish models and tumor infiltration and lysis using 3D coculture systems. We found that FAP regulates human NK cell migration, extravasation, and infiltration into matrix-containing tumors which ultimately affects tumor cell lysis. These findings demonstrate the necessity of proteolytic migration in NK cell function, suggest novel mechanisms of action of FAP targeting drugs, and provide an entirely new way to regulate NK cell activity.

Results

Human natural killer cells express catalytically active fibroblast activation protein (FAP)

We used pancreatic ductal adenocarcinoma (PDAC) as a model since it is characterized by extensive stroma that physically excludes immune cells (*24*). In PDAC, activated pancreatic stellate cells (PSCs) produce fibroblast activation protein (FAP) (*25*). We began by exploring the impact of NK cells on FAP expression by PSCs and cocultured primary PSCs with the human NK cell line NK92. Coculture of PSC with NK92 cells led to a four-fold increase in FAP activity compared to PSCs cultured alone as determined by a fluorescent peptide substrate FAP activity assay (Fig. 1A and Fig. S1A). However, this coculture experiment did not distinguish which cells produced the FAP (i.e. NK cells or PSCs). To address this, we cocultured PSCs with GFP expressing NK92 cells, FACS separated the two cell types and performed rt-qPCR for *FAP* expression in each cell population. Surprisingly, after 4 hours of coculture the PSCs possessed significantly reduced *FAP* expression, while the NK92 cells not only expressed *FAP*, but showed significantly increased *FAP* expression after coculture with PSCs (Fig. 1B and Fig. S1B).

Since NK cells are not known to produce FAP, we confirmed FAP expression at the protein level in NK92 cells and three additional human NK cell lines: NKL, YT and KHYG-1 (Fig. 1C and Fig. S1 C and D). To exclude the possibility that FAP expression was specific to NK cell malignancies, we assessed FAP expression in NK cells isolated from PBMCs of five different healthy human donors and found robust FAP expression in all donor NK cells (Fig. 1D and Fig. S1E). To determine if additional human immune cell types express FAP, we assessed multiple different human B, T and monocyte cell lines for FAP expression by western blot and found heterogeneous protein expression (Fig. 1E). This cell-line specific FAP protein expression was consistent with *FAP* mRNA expression as determined by analysis of RNAseq data derived

from the cancer cell line encyclopedia (*26*) (Fig. S1F). While we saw heterogeneous expression of FAP in B, T and monocyte cell lines, we did not detect FAP expression in healthy donor PBMC-derived B cells (CD19+), T cells (CD3+), and macrophages (CD14+) (Fig. 1F and Fig. S1G). Thus, FAP expression in non-NK cell lines is likely driven by their malignant biology, since FAP can be upregulated during the process of malignant transformation (*21*).

Canonically, FAP is surface-expressed, so we attempted to detect FAP by flow cytometry. Anti-FAP antibodies used for western blot failed to detect FAP on the positive control cell line (PSCs) (Fig. S2A-C). A polyclonal sheep anti-FAP antibody detected FAP on PSCs, but was unable to detect FAP on NK cells (Fig. 1G). This does not preclude the possibility that FAP is surface expressed on NK cells, but shows currently available anti-FAP antibodies are unable to detect FAP on the NK cell surface. To circumvent this, we turned to an antibody-independent means of detecting surface expression—surface protein biotinylation. We biotinylated cell surface proteins, and then excluded them from the cell lysate via magnetic separation. We then determined that FAP is present in total cell lysate but absent from the intracellular protein lysate (Fig. 1H), demonstrating that FAP is expressed on the NK cell surface. Due to the volume required to unbind biotinylated surface proteins from the magnetic beads, the surface protein lysate was too dilute to perform adequate western blot analysis (Fig. S2D). Faint bands of the appropriate size were observed when using the maximum volume (40 uL) the gel allowed (Fig. S2E). On NK cells, FAP may be structurally different or exist within a protein complex, rendering flow-based antibodies ineffective.

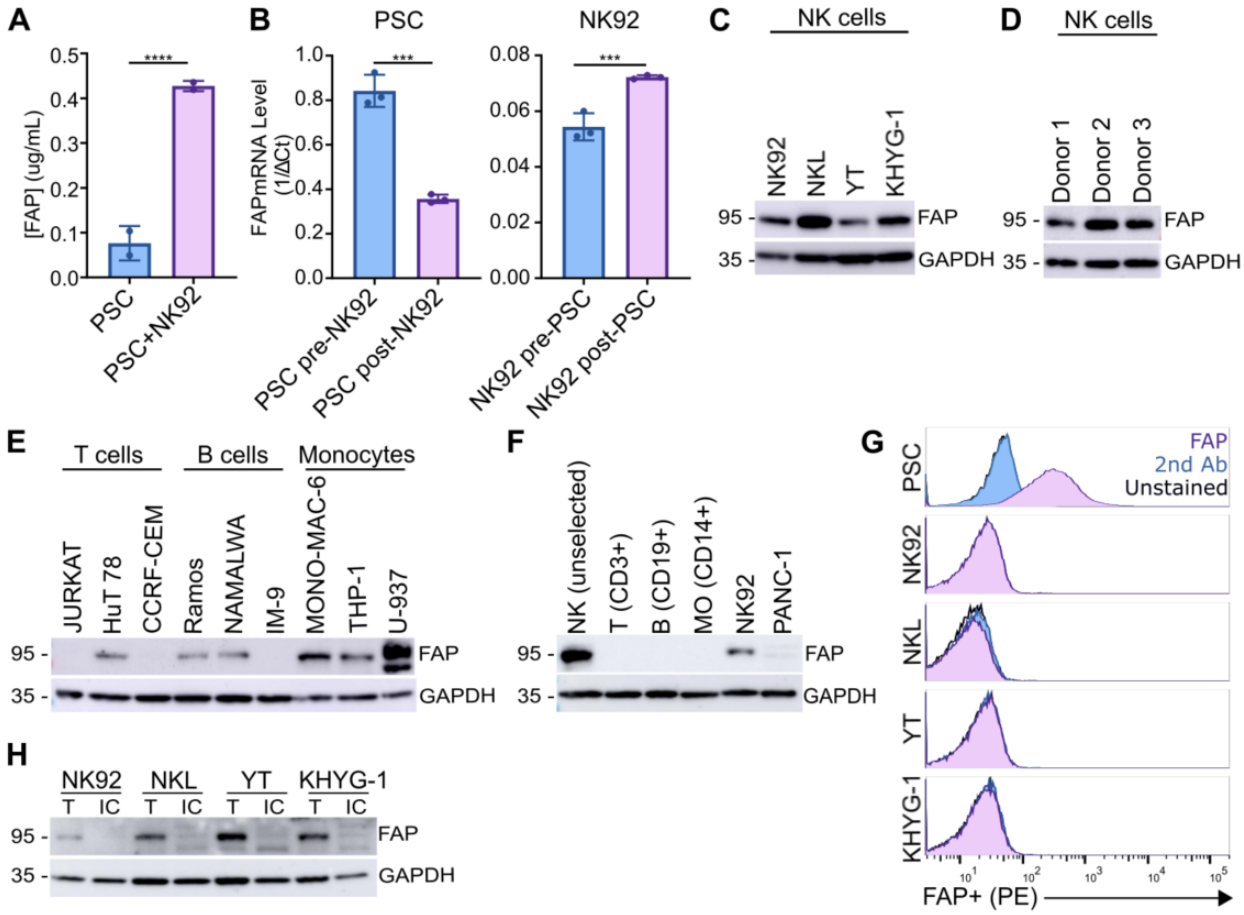

Fig. 1. Human NK cells express catalytically active fibroblast activation protein. (**A**) Fluorescent peptide substrate assay demonstrating 4-hour coculture of primary pancreatic stellate cells (PSC) with NK92 cells increases dipeptidyl peptidase activity. Results are from two independent experiments. (**B**) qRT-PCR analysis of *FAP* expression in PSCs and NK92 cells before and after coculture. Results are from three independent experiments. (**C**) Western blot showing that four distinct human NK cell lines express FAP. (**D**) Western blot showing primary NK cells isolated from PBMCs from three different healthy human donors express FAP. (**E**) Western blot showing heterogenous FAP expression in multiple human immune cell lines. (**F**) Western blot showing FAP is only expressed in human NK cells and not in human T (CD3+), B (CD19+) or monocyte (CD14+) cells. NK92 cell line

included as a positive control and PANC-1 cell line included as a negative control. Representative of results with two different donors. (**G**) Flow cytometry analysis assessing surface expression of FAP in human NK cell lines. Pancreatic stellate cells (PSC) included as a positive control. (**H**) Western blot of total protein (T) and intracellular (IC) protein isolated from human NK cell lines using cell surface protein biotinylation for exclusion of surface proteins. *P* value was calculated using unpaired two-tailed t-test. ***$P<0.001$, ****$P<0.0001$.

In NK cells, FAP gene expression correlates with extracellular matrix and migration regulating genes

To determine FAP's function in human natural killer cells we employed computational approaches. In 2011, Iqbal et al. performed a gene expression array on multiple NK cell lymphoma samples and NK cell lines (*27*). Using these data, we assessed FAP expression in 22 NK cell lymphomas and 11 NK cell lines (Fig. 2A) and performed a correlation analysis to assess the genes that were most positively and negatively correlated with FAP expression (Fig. 2B). The top 19 genes that were most positively correlated with FAP expression are shown in Figure 2C. We then performed GO enrichment analysis of these genes and determined that the pathways most positively correlated with FAP expression were related to extracellular matrix remodeling and cellular migration (Fig. 2D). This is consistent with the current understanding of FAP function, which is to cleave extracellular matrix components such as collagen and enhance cellular migration/invasion (*21*). It is also interesting that matrix metalloproteases (MMPs) were among the top 19 genes positively correlated with FAP expression. MMPs regulate rat, mouse

and human NK cell migration into collagen or Matrigel *in vitro* (*28–30*). These data suggest that FAP may also regulate NK cell migration.

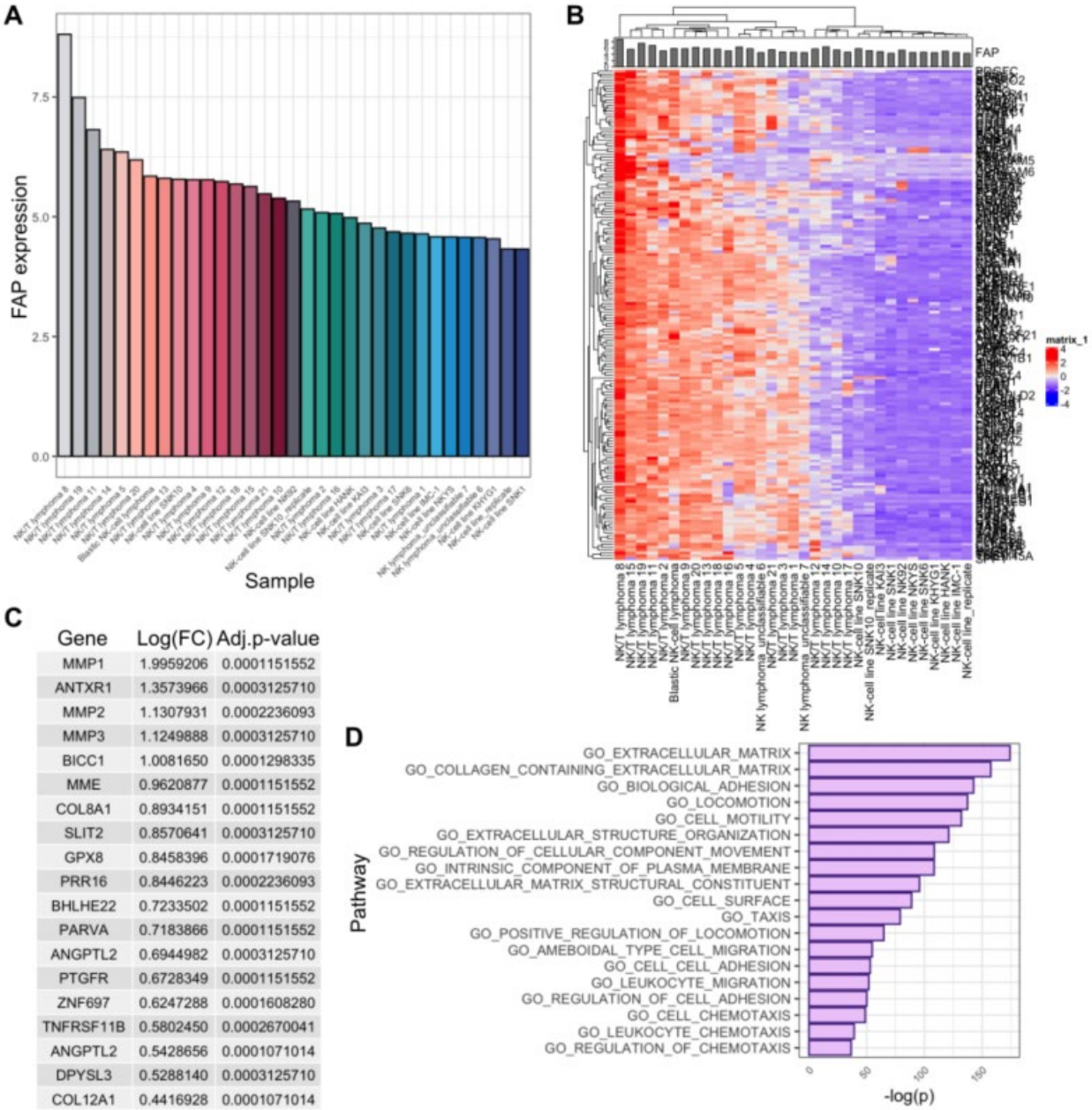

Gene	Log(FC)	Adj.p-value
MMP1	1.9959206	0.0001151552
ANTXR1	1.3573966	0.0003125710
MMP2	1.1307931	0.0002236093
MMP3	1.1249888	0.0003125710
BICC1	1.0081650	0.0001298335
MME	0.9620877	0.0001151552
COL8A1	0.8934151	0.0001151552
SLIT2	0.8570641	0.0003125710
GPX8	0.8458396	0.0001719076
PRR16	0.8446223	0.0002236093
BHLHE22	0.7233502	0.0001151552
PARVA	0.7183866	0.0001151552
ANGPTL2	0.6944982	0.0003125710
PTGFR	0.6728349	0.0001151552
ZNF697	0.6247288	0.0001608280
TNFRSF11B	0.5802450	0.0002670041
ANGPTL2	0.5428656	0.0001071014
DPYSL3	0.5288140	0.0003125710
COL12A1	0.4416928	0.0001071014

Fig. 2. In NK cells, FAP gene expression correlates with extracellular matrix and migration-regulating genes. (**A**) Level of FAP expression in NK cell lymphomas (n=22) and NK cell lines (n=11) as determined by Affymetrix gene expression array. (**B**) Heatmap of

gene expression array data. Data are shown as z-score scaled values. (**C**) Top 19 genes that are significantly correlated with FAP expression. (**D**) Top GO pathways that significantly correlate with FAP expression.

FAP inhibition reduces primary human NK cell migration

Based on the computational analysis, we hypothesized that FAP was expressed by human NK cells to enhance their migration. To test this hypothesis, we compared primary NK cell migration *ex vivo* in the presence and absence of a highly selective FAP-specific inhibitor — Cpd60. Cpd60 was designed to selectively inhibit FAP over other members of the prolyl oligopeptidase family S9. Cpd60's IC_{50} for FAP is 0.0032 uM versus >100 uM for DPP4, >12.5 uM for DPP9, >100 uM for DPP2 and >1.8 for PREP (prolyl oligopeptidase) (*31*). We confirmed Cpd60 inhibited FAP but not FAP's most closely related protein, DPPIV (Fig. 3A). Cpd60 had no effect on NK cell viability (Fig. S3A). To monitor NK cell migration we cocultured primary NK cells with EL08.1D2 cells, which have previously been shown to support spontaneous NK cell migration (*32*, *33*) and produce extracellular matrix (*34*), and live imaged them for 24 h capturing photos every 2 minutes (Fig. 3B). From these time-lapse videos we manually tracked NK cell migratory paths (Fig. 3C and D, Movie S1 and S2). These experiments were repeated with NK cells from three different donors, with similar results. We found that FAP inhibition with Cpd60 significantly reduced NK cell velocity (Fig. 3E) and the accumulated distance traveled by NK cells (Fig. 3F) but had no significant impact on the Euclidian distance — the straight-line distance between the starting point and end point (Fig. S3B) — traveled by NK cells (Fig. 3G).

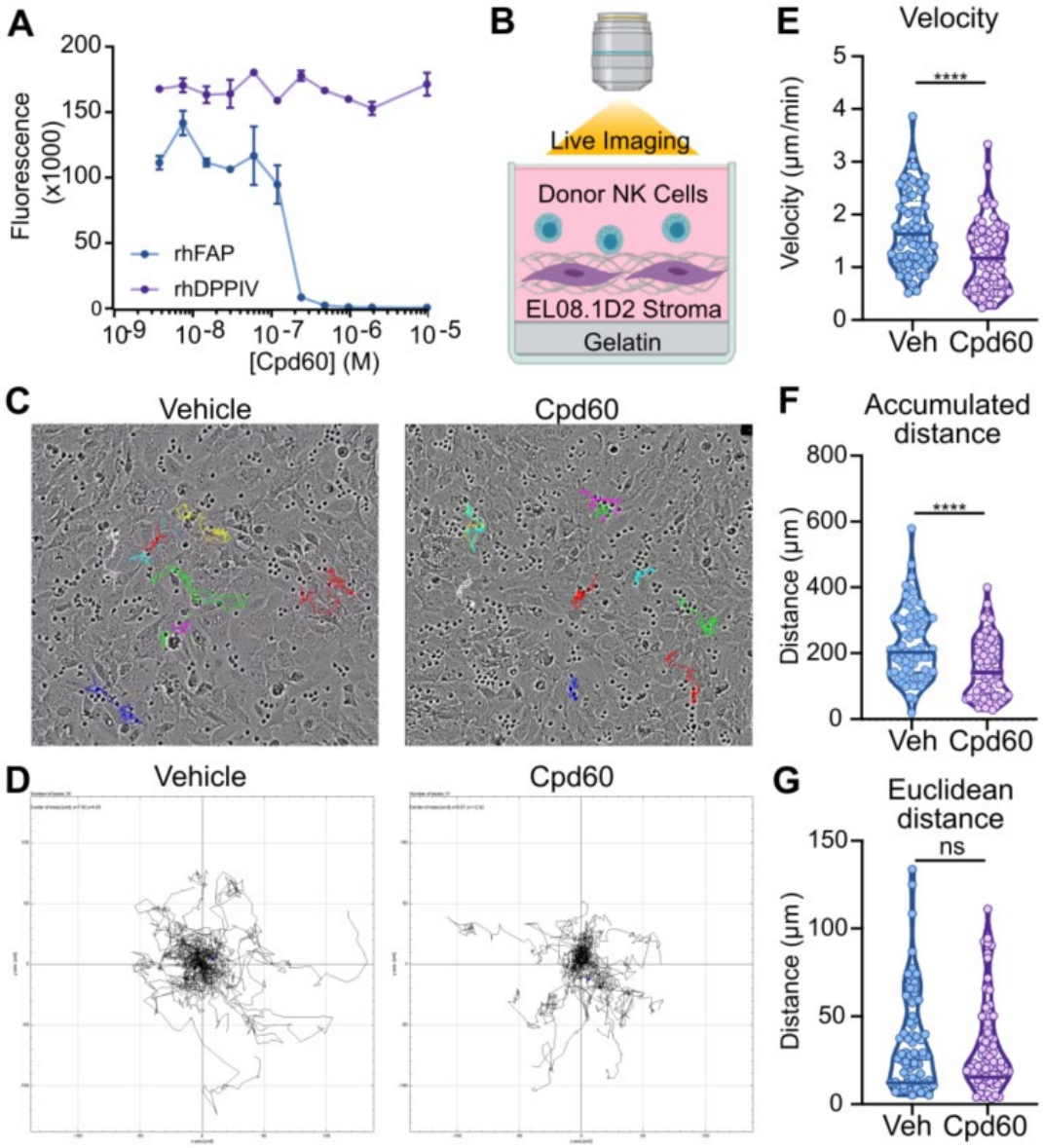

Fig. 3. FAP inhibition reduces primary human NK cell migration. (**A**) Fluorescent peptide dipeptidyl peptidase activity assay demonstrating FAP inhibitor (Cpd60) inhibits FAP but not DPPIV. (**B**) Schematic of live imaging of primary human NK cell migration on stromal cells. (**C**) Representative phase-contrast images from live imaging showing multiple colored tracks. Each color track represents the migration path of a single NK cell. (**D**) Rose plots with overlaid NK cell migration tracks. Each treatment group contains 30 different NK cells from a single healthy donor. (**E**) The average velocity, (**F**)

accumulated distance traveled and (**G**) Euclidian distance traveled by primary NK cells treated with either vehicle or 10 uM Cpd60. Each point represents a single NK cell. Each condition contains 90 NK cells with 30 NK cells from three separate donors.

FAP inhibition reduces NK cell extravasation in vivo

We next set out to determine if FAP altered NK cell migratory behaviors *in vivo*. Since we could not detect FAP expression in murine NK cells (Fig. S1H) we opted to use zebrafish—a novel *in vivo* model that allows us to monitor human NK cell migratory behaviors in real-time. We injected NK92-GFP cells into the pericardium of *Tg(kdrl:mCherry-CAAX)y171* zebrafish embryos that express endothelial membrane targeted mCherry (Fig. 4A). Immediately after injection, NK cells migrated via the circulation to the caudal hematopoietic tissue (Fig. 4B) hen gradually disseminating throughout the rest of the zebrafish vasculature. Using confocal live-imaging, which captured images approximately every 3 minutes, we captured an NK cell crawling along the inside of the blood vessel, searching for an appropriately sized pore just prior to extravasation (Fig. 4C and Movie S3, Fig. S4). After confirming that human NK cells could migrate throughout and extravasate from zebrafish vasculature, we tested the effects of FAP inhibition on NK cell extravasation. Since fluorescent microscopy is amenable to imaging multiple fish simultaneously, we used fluorescent microscopy to quantify the effects of the FAP inhibitor Cpd60 on NK cell extravasation. We confirmed that the fluorescent microscope was capable of detecting NK cell extravasation (Fig. 4D), and then imaged 20 fish injected with NK92-GFP cells, 10 of which were bathed in 10 uM of Cpd60, and 10 fish that were bathed in vehicle. Fish were imaged at 10X to visualize the entire fish. We found that FAP inhibition significantly reduced NK cell extravasation from the blood vessels (Fig. 4 E and F).

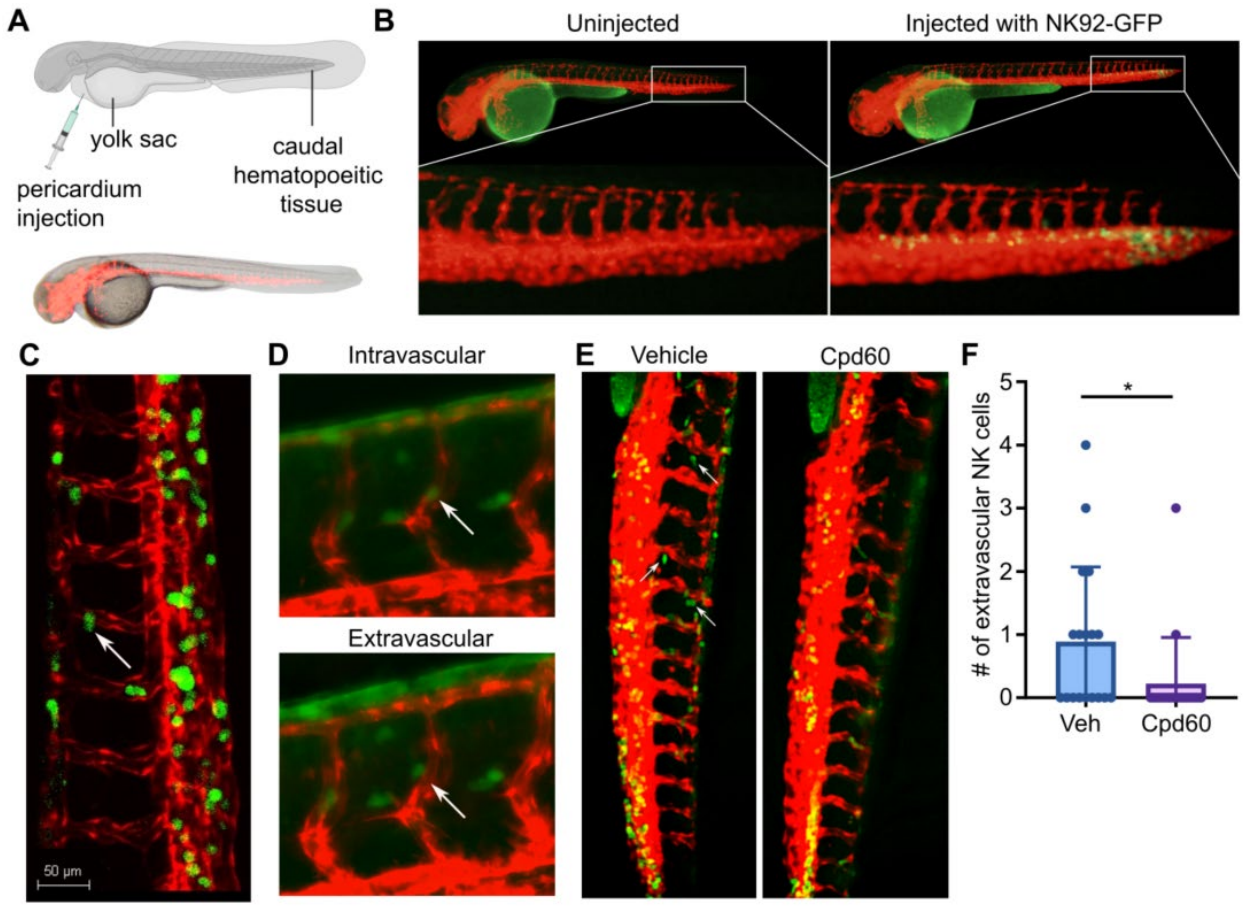

Fig. 4. FAP inhibition reduces NK cell extravasation from zebrafish blood vessels. (**A**) Schematic representation (top) of zebrafish injections. Fluorescent and brightfield overlay image of *Tg(kdrl:mCherry-CAAX)y171* zebrafish embryos expressing endothelial membrane targeted mCherry (bottom). (**B**) Representative images of caudal hematopoietic tissue immediately after NK92-GFP injection into the pericardium. (**C**) Still image taken from confocal time-lapse video demonstrating NK92-GFP extravasation from mCherry labeled vasculature. (**D**) Representative fluorescent microcopy images demonstrating NK92-GFP extravasation. Extravascular image was taken approximately 5 minutes after the intravascular image. Images were taken at 20X. (**E**) Representative

fluorescent microscopy images of NK92-GFP injected zebrafish in 10 uM FAP inhibitor (Cpd60) or vehicle showing NK92-GFP cell intravascular or extravascular localization 1 hour after injection. Images were taken at 10X. (**F**) Quantification of extravascular NK92-GFP cells in zebrafish injected with NK92-GFP cells 1 hour prior to imaging. *$p<0.05$ analyzed by unpaired two-tailed t-test. Data are aggregated from two independent experiments, each with 10 fish per treatment condition and quantification was done blinded to treatment conditions.

FAP inhibition reduces NK cell infiltration into matrix containing PDAC tumor spheroids

NK cells regulate tumor growth and viability, yet the mechanisms NK cells employ to migrate through dense tumor-related extracellular matrix is unknown. To determine if FAP activity affects NK cell infiltration into tumors we used tumor spheroid models of PDAC generated from the PDAC cell line PANC-1 and primary pancreatic stellate cells (PSCs, PSCs comprise the majority of cancer-associated-fibroblasts in PDAC tumors). Homogeneous PANC-1 tumor spheroids have minimal extracellular matrix but PSC and PSC+PANC-1 heterogeneous tumor spheroids contain rich stroma that contains extracellular components such as collagen and fibronectin (*35*, *36*). We generated homogenous PANC-1 or PSC spheroid and heterogeneous PANC-1+PSC spheroids by plating 10,000 cells in a 0.1% agarose coated U-bottom plate and allowed the spheroids to form over 24 hours. After 24 hours, 1,000 NK92-GFP cells were added to the spheroids and 4 hours later the spheroid-NK cell cocultures were imaged using fluorescent microscopy. To assess the extent of NK cell infiltration into tumor spheroids, we measured GFP intensity along an equatorial line drawn from the surface of the spheroid in FIJI. The line drawn for each spheroid was the same length. We then divided this line into quarters, which we termed

“edge”, “mid-edge”, “mid-center” and “center”, then averaged the intensity along those quarters (Fig. 5A).

As expected, NK cells infiltrated into PANC-1 spheroids more readily than they infiltrated PSC spheroids (Fig. 5B and C). This is likely because PANC-1 spheroids do not contain extracellular matrix like PSC spheroids; PANC-1 spheroids thus lack the physical matrix barrier that impedes NK cell infiltration. We next assessed the impact of FAP inhibition on NK cell infiltration into homogenous PANC-1 spheroids, homogenous PSC spheroids, and heterogeneous PANC-1+PSC spheroids (Fig. 5D, E and F). We found that 10 uM Cpd60 significantly reduced NK cell content in the mid-edge and mid-center regions of the PSC spheroids, and significantly reduced NK cell content in the mid-edge region of the PSC+PANC-1 spheroids, yet had no effect on NK cell content in any region of the PANC-1 spheroids. These results suggest that FAP regulates NK cell migration through tumors, but only in the presence of extracellular matrix.

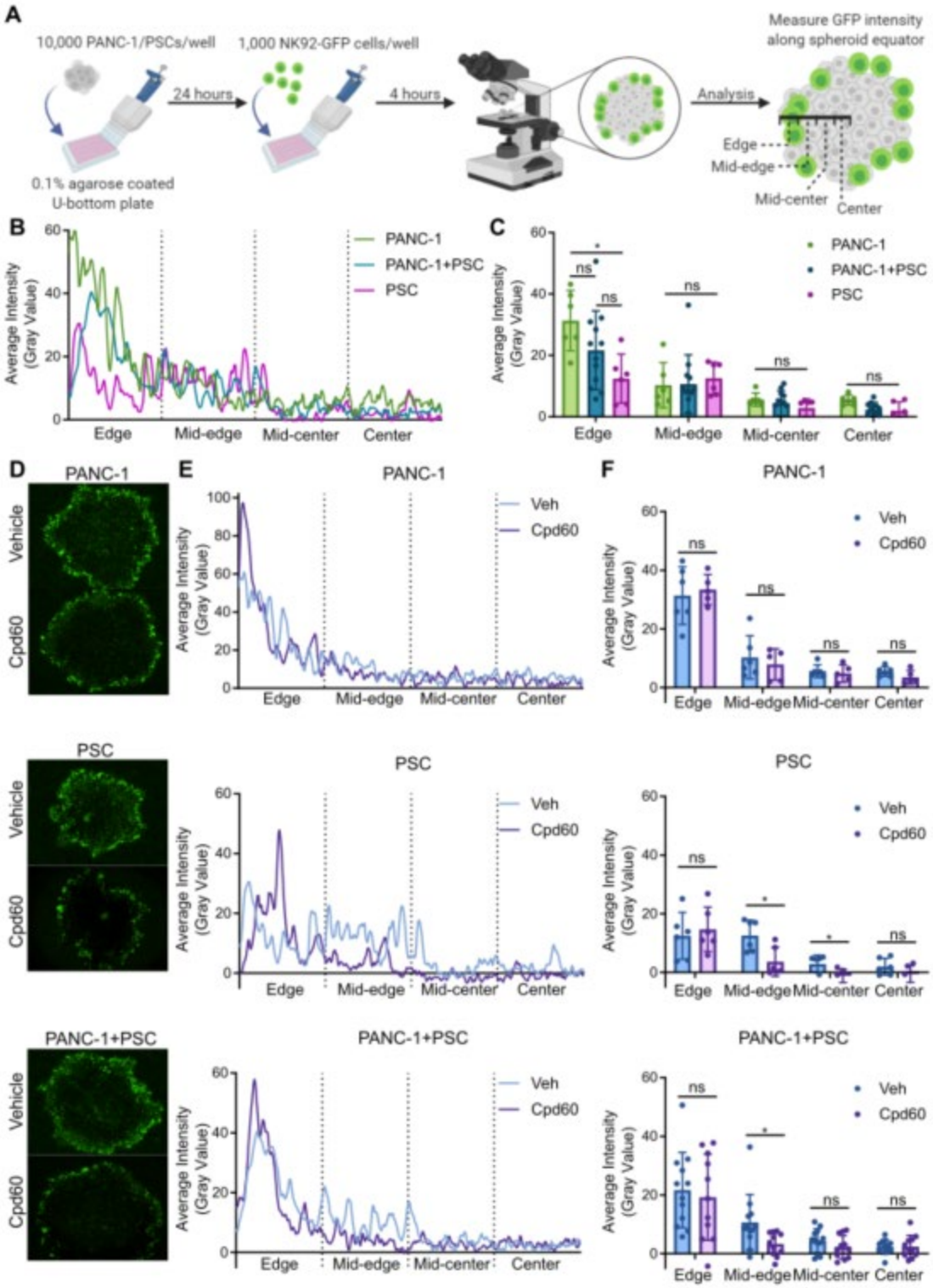

Fig. 5. FAP inhibition reduces NK cell infiltration into matrix containing spheroids. (**A**) Schematic representation of experimental methods and analysis. (**B**) Average continuous

GFP intensity measured along PANC-1, PSC or PANC-1+PSC spheroid equator. (**C**) Average GFP intensity in the edge, mid-edge, mid-center and center regions of PANC-1, PSC and PANC-1+PSC spheroids. PANC-1 n = 6; PSC n = 6; PANC-1+PSC n=12. *p<0.05 as determined by ordinary one-way ANOVA followed by Tukey's multiple comparison test. (**D**) Representative fluorescent images of NK92-GFP cells infiltrating into tumor spheroids cultured in vehicle or 10 uM FAP inhibitor (Cpd60). (**E**) Average continuous GFP intensity measured along PANC-1, PSC or PANC-1+PSC spheroid equator cultured in vehicle or 10 uM Cpd60. (**F**) Average GFP intensity in the edge, mid-edge, mid-center and center regions of PANC-1, PSC or PANC-1+PSC spheroids cultured in vehicle or 10 uM Cpd60. PANC-1+vehicle n = 6; PANC-1+Cpd60 n=5; PSC+vehicle n = 6; PSC+Cpd60 n=6; PANC-1+PSC+vehicle n=12, PANC-1+PSC+Cpd60 n=12. *p<0.05 as determined by unpaired two-tailed t-test.

FAP inhibition reduces NK cell infiltration into and lysis of PANC-1 cell clusters embedded in matrix

While the spheroid experiments shown in Figure 5 suggest that FAP inhibition reduces NK cell migration through a tumor-associated extracellular matrix, interpretation of these results was constrained because the pancreatic stellate cells (PSCs) incorporated into the tumor spheroids to produce matrix also express FAP. Therefore, we could not exclude the possibility that FAP inhibition reduced NK cell infiltration into tumor spheroids by inhibiting the FAP activity of PSCs. To address this issue, we assessed the effect of FAP inhibition on NK cell infiltration into PANC-1 clusters embedded in matrix. These culture systems did not contain PSCs; the only FAP expressing cells present were the NK cells. We also investigated the effect

of FAP inhibition on NK cell infiltration into PSC clusters embedded in matrix. To accomplish this, we plated 1,000 PANC-1 or PSCs in low-adhesion U-bottom plates and allowed them to form clusters for 24 hours. We then embedded the clusters in matrix that consisted of 80% collagen/20% Matrigel and NK92-GFP cells, and added either 10 uM Cpd60 or vehicle to the media. We live imaged the cocultures for 24 hours, capturing images every 30 minutes. Then we fixed the slides and stained for GFP by immunofluorescence to quantity the amount of NK cell infiltration into the clusters (Fig. 6A). FAP inhibition had no effect on cluster size (Fig. S5A). FAP inhibition significantly reduced NK92-GFP cell infiltration into PANC-1 and PSC clusters embedded in matrix (Fig. 6B and C, Movies S4-7). To determine if this reduced NK cell infiltration was accompanied by reduced tumor cell lysis we repeated the PANC-1 and NK92 coculture experiment and stained the cells for actin using phalloidin and cleaved caspase 3 to identify apoptotic cells. Using the phalloidin stain we outlined the PANC-1 cell cluster, and then transposed the outline onto the cleaved caspase 3 images and quantified the intensity of cleaved caspase 3 within PANC-1 cell clusters (Fig. 6D). We found that FAP inhibition significantly reduced the amount PANC-1 cell apoptosis (Fig. 6E) in 3D cultures, despite having no effect on PANC-1 cell apoptosis in 2D cell cocultures (Fig. S5B). To determine if FAP inhibition also reduced donor NK cell migration and tumor lysis, we repeated these experiments with NK cells from two donors. Since the range of PANC-1 cluster areas in the donor NK cell experiment was much wider than the range in the NK92 experiment (10-208 versus 12-70) we normalized the intensities in the donor NK cell experiment to the area of the cluster. In agreement with the NK92 cell experiments, FAP inhibition reduced donor NK cell lysis of PANC-1 cells in 3D (Fig. 6E) but not 2D (Fig. S5B). This demonstrates that FAP inhibition does not alter target cell lysis

through direct impacts on NK cell cytotoxicity but rather via modulation of NK cell migration through matrix.

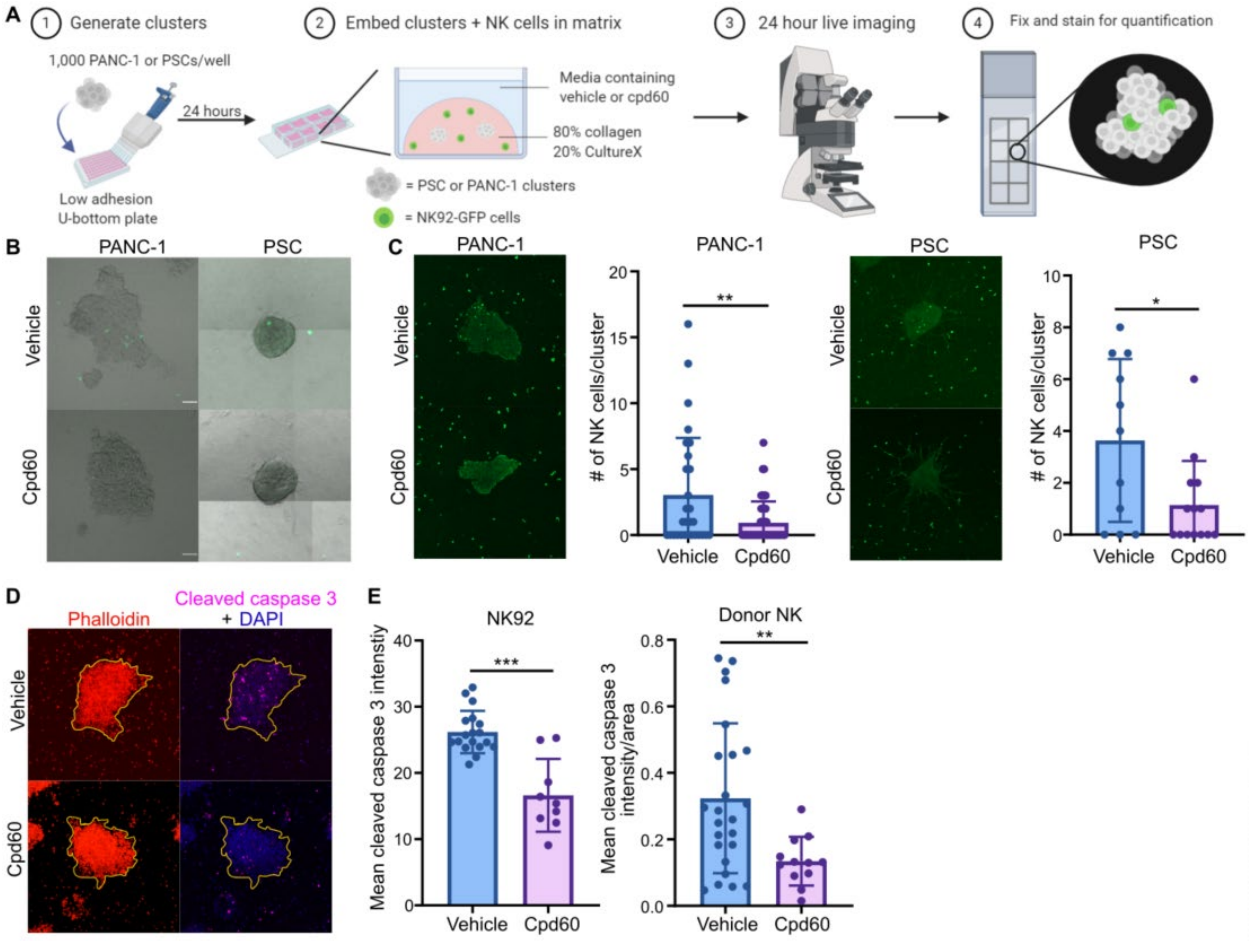

Fig. 6. FAP inhibition reduces NK cell infiltration and lysis of PANC-1 cell clusters embedded in 3D cell matrix. (**A**) Schematic representation of experimental design. (**B**) Still images from confocal time-lapse video 24 hours after coculture of NK92-GFP with PANC-1 or PSC clusters embedded in 3D matrix and vehicle or 10 uM FAP inhibitor (Cpd60). (**C**) Representative immunofluorescence images and quantification of NK92-GFP cell infiltration into PANC-1 or PSC clusters after 24-hour coculture with vehicle or 10 uM Cpd60. PANC-1+vehicle n = 29; PANC-1+Cpd60 n=45; PSC+vehicle n = 11; PSC+Cpd60 n=14. PANC-1 data aggregated from two independent experiments. (**D**)

Representative immunofluorescence images of phalloidin and cleaved caspase 3 staining in PANC-1 cell clusters cocultured with NK92 and vehicle or 10 uM Cpd60. (**E**) Quantification of cleaved caspase 3 intensity staining in PANC-1 cell clusters cocultured with NK92 cells or donor NK cells. PANC-1+NK92+vehicle n = 18; PANC-1+NK92+Cpd60 n = 9; PANC-1+Donor NK+vehicle n=25, PANC-1+Donor NK+Cpd60 n =12. Donor NK cell data is aggregated data from two independent experiments that used different donors. *$p<0.05$, **$p<0.01$, ***$p<0.001$ as determined by unpaired two-tailed t-test.

Discussion

Here we show human natural killer (NK) cells express FAP, which regulates NK cell migration, extravasation and tumor infiltration. This observation adds to current understanding of NK cell migration and tissue infiltration, and describes a mechanism for NK cell extravasation from blood vessels. We additionally show that reduced tumor infiltration reduces tumor cell lysis, confirming the importance of FAP-based migratory mechanisms for the anti-cancer activity of NK cells. Therefore, this work reveals novel insights into FAP biology and NK cell biology and has important implications for emerging NK cell-focused therapeutic strategies.

For extravasation or tissue invasion, cells must penetrate the basement membrane and interstitial tissue. During this process they are confronted by 3D extracellular matrix (ECM) that provides a substrate for adhesion and traction, as well as biomechanical resistance. In order for cells to traffic effectively through the ECM, which can offer narrow or non-existent pores for passage, leukocytes must adopt contracted shapes. Excessive cellular deformation can result in nuclear rupture that causes genomic damage, long-term genomic alterations and limited cellular

survival. To circumvent nuclear damage, some cells employ proteolytic digestion to widen pores in the ECM (*20*). Although proteolytic migration is considered less common in leukocytes versus other cell types, it has been documented. Zebrafish neutrophils and macrophages use proteolytic digestion for basement membrane transmigration (*37*). Human neutrophils secrete elastase, a serine protease, to facilitate their endothelial transmigration (*38*).

In comparison to other immune cell types, there are few studies investigating the physical mechanisms driving NK cell migration. Decades-old research demonstrated that mouse and rat NK cell migration through Matrigel was dependent on matrix metalloproteinases (MMPs) (*29*, *39*, *40*). More recent studies have used more physiologic models. Putz et al. showed that heparinase regulated mouse NK cell infiltration into murine tumors (*41*). Prakash et al. showed that granzyme B released from murine cytotoxic lymphocytes, including NK cells, enhanced lymphocyte extravasation via ECM remodeling, although it did not affect interstitial migration. They confirmed that a granzyme B inhibitor reduced human donor T cell transmigration through a Matrigel coated semi-permeable membrane (i.e. Boyden chamber assay) (*42*). Although these authors did not assess changes in human donor NK cell migration in response to a granzyme B inhibitor, it is reasonable to assume it would be similar to that of T cell migration since both cell types express and release granzyme B. However, our finding that FAP is expressed exclusively in human NK cells, and not in murine NK cells or other human immune cell types (Figure 1), suggests that some migratory mechanisms can be cell-type and species-specific. Unlike these previous studies that investigated either extravasation or tumor infiltration, we investigated both and found that NK cells use the same proteolytic migration strategy for basement membrane degradation/extravasation as well as tumor tissue infiltration. We further prove that defects in proteolytic migration directly impair the ability of NK cells to lyse malignant cells.

FAP is a well-studied protein. Although once thought to be restricted to activated fibroblasts, FAP expression has been found in additional cell types such as epithelial tumors (*43–45*), melanocytes (*46*) and macrophages (*47*, *48*). In non-immune cells, FAP enhances cellular invasion (*46*, *49–52*). The role of FAP in macrophages is less clear. Arnold et al. showed that in murine tumors there is a FAP+ minor sub-population of immunosuppressive F4/80^{hi}/CCR2^{+}/CD206^{+} M2 macrophages. While this study highlighted how FAP+ macrophages affect tumor growth, FAP's function in these macrophages was not described (*47*). Tchou et al. identified FAP+CD45+ cells in human breast tumors by immunofluorescence. They then used flow cytometry to demonstrate that some of these FAP+CD45+ cells were CD11b+CD14+MHC-II+ tumor associated macrophages. Since the flow cytometry panel used to categorize these FAP+CD45+ cells consisted of only macrophage markers, those data do not exclude the possibility that some of the FAP+CD45+ tumor cells were NK cells. In contrast to that study, we did not identify FAP expression in human macrophages (CD14+ cells) (Figure 1F). However, we examined circulating cells, as opposed to cells in the tumor microenvironment. Future studies are needed to further categorize FAP expression in tumor immune cell populations, presumably using multicolor immunofluorescent staining, since we were unable to detect FAP expression by NK cells using cell surface-based flow cytometry approaches. Additionally, more studies are needed to determine the function of FAP in these FAP+ tumor macrophages to determine if it enhances proteolytic migration similar to FAP's function in NK cells which we described here.

The findings that human NK cells express FAP (Figure 1D) has several clinical implications for FAP-targeted therapies. For example, an anti-FAP/IL-2 fusion protein is currently in clinical trials (NCT02627274). The proposed mechanism of action of this drug is that it targets IL-2 to FAP expressing tumor stroma, thereby limiting on-target, off-site toxicities

associated with IL-2 cytokine therapy. Our findings that FAP is expressed on the NK cell surface suggests that and anti-FAP/IL-2 fusion protein may also target IL-2 directly to NK cells, enhancing NK cell activation and potentially tumor clearance. Since we were unable to detect FAP on the NK cell surface by flow cytometry, it is plausible that the anti-FAP construct in the anti-FAP-IL-2 fusion protein targets a similar epitope as the anti-FAP antibody we used, and therefore would not target IL-2 to NK cells. Our inability to detect FAP on NK cells by flow may be a byproduct of masked epitope or altered FAP structure, which would render nearly all anti-FAP antibodies unusable. Alternatively, this may be an antibody-specific problem and other anti-FAP antibodies would bind FAP on NK cells. Future studies are needed to determine if the anti-FAP/IL-2 fusion protein currently in clinical trials can bind to FAP on the NK cell surface.

Anti-FAP CAR therapies are also in development to treat conditions such as cardiac fibrosis (*22*), malignant pleural mesothelioma (*53*), lung adenocarcinoma (*54*) and other cancers (*55*). Our data suggest that anti-FAP CAR cells may also be useful in NK cell malignancies such as aggressive NK-cell leukemia if the anti-FAP portion was able to bind FAP on NK cells. There are potential caveats to the clinical use of anti-FAP CAR T cells. In one study, anti-FAP CAR T cells failed to regulate murine tumor growth and induced lethal bone toxicity and cachexia, potentially through the lysis of multipotent bone marrow stromal cells (*56*). It is plausible that an anti-FAP CAR T cell could induce NK cell lysis, resulting in NK cell leukopenia in humans only, therefore this toxicity would be missed in preclinical murine models. For cancer immunotherapy, an ideal anti-FAP CAR would be engineered to target FAP expression by fibroblasts and spare NK cells. Our findings that the anti-FAP antibody we used had variable binding to fibroblasts (i.e. PSCs) versus NK cells suggest this type of anti-FAP CAR engineering is feasible. It should be noted that Gulati et al. performed the first-in-human trial of an anti-FAP

CAR T cell therapy, and demonstrated that a FAP CAR T cell therapy induced stable disease for 1 year in a patient with malignant pleural mesothelioma without any treatment-terminating toxicities (*53*).

Our findings that FAP regulates NK cell tissue infiltration (Figures 5 and 6) has clinical implications. FAP inhibitors, such as Cpd60, could reduce NK cell infiltration into tissues in diseases characterized by excessive NK cell content. These results also imply the potential value of engineering NK cells that overexpress FAP, enhancing NK cell tumor infiltration, which in turn would enhance tumor cell lysis.

Other strategies aimed at enhancing NK cell infiltration into tumors rely on manipulating chemokine/receptor pathways. One approach is to process NK cells in such a way that they have enhanced migratory phenotypes. For example, Wennerberg et al demonstrated that *ex vivo* expanded NK cells express higher levels of chemokine receptor CXCR3 than unexpanded NK cells. The expanded NK cells in turn had increased migration towards CXCL10 expressing melanomas (*18*). They suggested that autologous NK cell therapy could be improved by expanding the NK cells prior to reinjection to enhance tumor homing. Another approach is to engineer NK cells to enhance their migration. Kremer et al engineered NK cells to overexpress CXCR2, a chemokine receptor. They showed that CXCR2 overexpressing NK cells had enhanced trafficking towards and lysis of renal cell carcinoma cells *in vitro* (*19*). These findings suggest that strategies to enhance NK cell migration are both feasible and may have clinical applicability. However, chemokine pathway-altering strategies have built-in limitations. They require not only elevated expression of the chemokine receptor on NK cells, but also secretion and maintenance of chemoattractants by the tumor. Additionally, many chemoattractants recruit multiple immune cell types, including immunosuppressive cells. For example, CXCL10 is a

chemoattractant for cytotoxic T lymphocytes and NK cells, but also for regulatory T cells (*57*). We postulate that the ideal migration-altering therapeutic approach would increase cytotoxic immune cell infiltration in tumor masses, without influencing or even reducing immunosuppressive immune cell content in the TME. Since inhibiting FAP reduces NK cell tumor infiltration and lysis (Figure 6), we therefore speculate that the inverse is true and that engineering NK cells to overexpress FAP, either in autologous NK cell or CAR-NK therapies, could increase NK cell tumor infiltration and lysis. This approach is independent of tumor-associated factors, such as chemoattractant secretion, and would not be expected to induce the infiltration or expansion of immunosuppressive cell populations into the tumor microenvironment. Since proteolytic migration is required for NK cell killing of malignant cells (Figure 6), the ability to alter protease expression or activity to enhance NK cell tumor infiltration represents a potentially promising approach to altering NK cell anti-tumor activity. Future studies are needed to explore the benefit of FAP-overexpressing NK cells in preclinical models and in clinical studies, and to determine what, if any, toxicities they induce.

This work also demonstrates the feasibility of studying human NK cell migration using physiologically relevant approaches in model systems. Human immune cell intravasation/extravasation studies often rely on artificial endothelial cell membranes. By using a zebrafish model, we were able to visualize and quantify human NK cell extravasation *in vivo* (Figure 4). Van den Berg et al. demonstrated zebrafish models could be combined with advanced microscopy techniques, such as correlative light and electron microscopy, to visualize zebrafish immune cell extravasation (*37*). We have built upon this work and demonstrated that human NK cells can be inoculated into zebrafish embryos without apparent toxicities to the cells or the fish. We believe this model fills a current gap in available methodologies to investigate human

immune cell migratory phenotypes *in vivo*. We also demonstrated that heterotypic spheroids, comprised of stromal producing cells and cancer cell lines, can be used to assess the impact of tumor matrix on immune cell migration (Figure 5) complementing the less physiologic yet more controllable approach of embedding cells in 3D matrices.

The FAP functional studies described here would be improved with the application of FAP knock out NK cells. Because the generation of knock out NK cells is technically challenging, we believe the specific small molecule FAP inhibitor, Cpd60, represents a reasonable alternative to genetic knockout and also demonstrates that small molecules targeting FAP can alter NK cell function (Figures 3-6).

In this study we have demonstrated that human NK cells express FAP and FAP directly affects NK cell migration, extravasation and tumor infiltration. These findings further the understanding of FAP biology and NK cell migration strategies. These results have meaningful implications for FAP-targeting therapies currently in development and represent novel mechanisms that can be exploited to alter NK cell biology for clinical benefit.

Materials and Methods

Cell pellets, lines and culture

Primary human PSCs (ScienCell, cat#3830) were maintained on plastic and passaged every 1-3 days in stellate cell medium (ScienCell, cat#5301). For all experiments, PSC passage 5-9 was used. All human NK cell lines (NK92, NKL, YT and KHYG-1) and murine NK cell lines (LNK) were kindly provided by Dr. Kerry S. Campbell (Fox Chase Cancer Center, Philadelphia, PA). The NK92-GFP expressed GFP due to nucleofection with pmaxGFP according to manufacturer's protocol (Lonza, cat#VVCA-1001). All NK cell lines were cultured as previously described (*58*), tested for mycoplasma every 3-6 months and fingerprinted annually. (NKL could not be fingerprinted because it has no published profile). PANC-1 cells were cultured in 10%FBS in DMEM. The cell pellets of cell lines tested for FAP expression by western blot (Jurkat, HuT 78, CCRF-CEM, Ramos, Namwala, IM-9, mono-mac 6, THP-1, U-937, Swiss3T3, RAW264.7, JAWSII, P815, BW5147.3, EL4 and A-20) were obtained from the Georgetown Lombardi Comprehensive Cancer Center Tissue Culture Shared Resource.

Healthy donor derived cells

Fresh healthy donor NK cells were purchased from AllCells with either CD56 positive selection or CD56 negative selection (Allcells, cat#PB012-P or PB012-N). For 2D migration experiments, NK cells were enriched from peripheral blood using RosetteSep (StemCell Technologies) from healthy adult donors. T cells, B cells and monocytes were isolated from PBMCs (Allcells) using Mojosort magnetic cell separation system from Biolegend via CD3 positivity (Biolegend, cat#480133), CD19 positivity (Biolegend, cat#480105), CD14 positivity (Biolegend, cat#480093). PBMC purity was assessed using flow cytometry: CD3-APC (Biolegend, cat#300411), CD14-BV421 (Biolegend, cat#325627), CD45-FITC (BD Bioscience,

cat#347463), CD56-PE (BD Bioscience, cat#555516), CD20-PE (BD Bioscience, cat#555623). For donor NK cell lysis of PANC-1 clusters, primary donor NK cells were purchased from Allcells then expanded using irradiated K562-4-1BBL-mbIL-21 (names "CSTX002") cells kindly provided by Dr. Dean Lee according to his protocol (*59*).

FAP Activity Assay

One day prior to assay, 5,000 PSCs/well were added to 96 well flat clear bottom white polystyrene TC-treated microplates (Corning, cat#3610). The following day, PSC media was aspirated off and 50 uL of NK92 cells (lacking GFP) were added to each well containing PSCs at a 4:1 E:T ratio and incubated overnight at 37°C. 100 mM stock of dipeptidylpeptidase substrate (Acetyl-Aka-Gly-Pro-AFC) (Anaspec, CatAS-24126) was made by resuspending lyophilized substrate in DMSO. On the day of the assay, DMSO stock was then diluted 1:1000 in FAP activity assay buffer (50 mM Tris-BCl, 1 M NaCl, 1 mg/mL BSA, pH 7.5). A standard curve was generated using rFAP (R&D systems, 3715-SE-010). 50 uL of rFAP standard was added to wells in triplicate. 50 uL of substrate was added to each well and the plate was incubated for 5 minutes at 37°C. The plate was read on a PerkinElmer EnVision Multimode Plate Reader with 390-400 nm excitation and 580-510 nm emission wavelengths. The final concentration of FAP per well was calculated using the standard curve. Data were compiled and assessed for statistical significance using GraphPad Prism 9.

PSC-NK92 Coculture Assay

PSCs were plated one day prior to assay at 100,000 cells/well in a 6 well collagen coated plate. NK92 cells were added at 1:1 or 4:1 effector to target (E:T) ratios and cocultured for 3-4 hours. Each well contained 50% v/v NK and PSC media and 1% v/v IL-2. Following incubation, nonadherent cells were collected. Adherent cells were washed 2X with PBS and then trypsinized

with 0.05% trypsin. After detachment trypsin was quenched with equal volume PSC media and cells were collected, pelleted and washed 2X with PBS then resuspended in 600 uL of 1% BSA. Cells were immediately sent for nonsterile flow sorting of GFP+ from GFP- using the BD FACS Aria Ilu cell sorter in the Georgetown Lombardi Comprehensive Cancer Center Flow Cytometry and Cell Sorting Shared Resource (FCSR).

RNA Isolation and rt-qPCR

RNA was isolated using the PureLink RNA Mini Kit (Ambion, cat#12183020). The RNA concentration was measured using NanoDrop 8000 (Thermo Fisher Scientific). cDNA was generated from 20-100 ng of RNA using the GoTaq 2-step RT-qPCR System (Promega, cat# A6110). qPCR was performed with SYBR Green on a StepOnePlus real-time PCR system (Applied Biosystems). Gene expression was normalized to HPRT and analyzed using 1/ΔCt method.

Primers sequences:

FAP (F: ATGAGCTTCCTCGTCCAATTCA; R: AGACCACCAGAGAGCATATTTTG)

HPRT: (F: GATTAGCGATGATGAACCAGGTT; R: CCTCCCATCTCCTTCATGACA)

Western Blot

Western blots were performed as previously described (*58*). Western blots were conducted using anti-FAP (ab207178, abcam) at concentrations of 1:1000 diluted in 5% milk in PBST. Secondary antibody was anti-rabbit IgG, HRP linked (Cell Signaling, cat# 7074S) at 1:1000. Antibody was validated with additional anti-FAP antibodies (MyBiosource, cat#MBS303414 and abcam, car#ab53066). GAPDH antibody (Cell Signaling, cat#5174S) was used at 1:10,000. The secondary antibody was anti-rabbit IgG, HRP linked (Cell Signaling) used

at 1:5000. Chemiluminescent substrate (Pierce, cat#32109 or cat#34094) was used for visualization.

FAP Flow Cytometry

Cell pellets were collected via centrifugation at 1000rpm for 5 mins. Cells were washed 2X with 1XPBS and resuspended in 100 uL staining buffer (1%BSA in PBS). To test western blot anti-FAP antibodies, first 5 uL of anti-FAP antibody was used (either ab207178 or ab53066) incubated for 30 min at 4 degrees in the dark then washed twice with staining buffer. Then 2 uL of secondary antibody (Goat F(ab')2 Anti-Rabbit IgG(H+L) Alexa Fluor 647 (southern biotech, cat# 4052-31)) was added, incubated for 30 min at 4 degrees in the dark then washed twice with staining buffer. After this failed to work we removed the need for secondary antibody by conjugating ab207178 to APC using a lightning link conjugation kit (abcam, cat#ab2018071). Various concentrations of ab207178-APC antibody were tested. For successful flow, 1 uL of human Fc block (BD Pharmingen, cat#564219) was added and incubated at 4˚C for 45 minutes. 4 uL of 0.25 mg/mL sheep anti-human FAP antibody (R&D systems, cat#AF3715) or 0.5 uL of 2 mg/mL sheep IgG control (R&D systems, cat#5-001-A) was added and cells incubated at 4˚C for 30 minutes, vortexing half way through. Cells were washed 2X with staining buffer then resuspended in 100 uL staining buffer. 2 uL of PE-conjugated donkey anti-sheep secondary was added (R&D systems, cat#F0126) and incubated at 4˚C for 30 minutes in the dark, vortexing half way through. Cells were washed 2X with staining buffer then resuspended in 600 uL staining buffer. Samples were run in the Georgetown Lombardi Comprehensive Cancer Center Flow Cytometry Cell Sorting Shared Resource using BD LSRFortessa. Analyses were performed using FlowJo (v10.4.1).

Cell Surface Biotinylation

Cell surface biotinylation of NK92, NKL, YT and KHYG-1 cells was performed with the Pierce Cell Surface Protein Isolation kit (Thermo Scientific, cat#89881) according to the manufacturer's protocol. In brief, $4x10^8$ cells were pelleted and washed with cold PBS then incubated with EZ-LINK Sulfo-NHS-SS-biotin for 30 min at 4°C followed by the addition of a quenching solution. Another $1X10^6$ cells were collected and saved for total cell western blotting. Cells were lysed with lysis buffer (500 µL) containing the cOmplete protease inhibitor cocktail (Roche, cat#11697498001). The biotinylated surface proteins were excluded with NeutrAvidin agarose gel (Pierce, 39001). Samples were diluted 50 ug in ultrapure water supplemented with 50 mM DTT. Lysates were subjected to Western blotting with the anti-FAP antibody described above.

Computational analyses

NK lymphoma and cell line gene expression was downloaded from GEO (GEO accession GSE19067) (*27*) using R version 3.6.2 and read using affy in Bioconductor (*60*). Non-NK cell samples were excluded from analysis. Heatmap was created using ComplexHeatMap version 2.1.1 (*61*). Correlation analysis was performed using limma in Bioconductor (*62*). Gene set enrichment analysis was performed using GO enrichment (*63*).

2D NK migration studies

2D migration studies were done as previously reported (*33*, *34*). In brief, EL08.1D2 stromal cells were grown to a confluent monolayer on flat-bottomed 96 well ImageLock plates (Essen Bioscience) pre-coated with 0.1% gelatin (Stemcell Technologies). 10 uM of Cpd60 in RPMI media was added to the chamber 15 min before imaging. Freshly isolated human NK cells were imaged in 96-well on the IncuCyte ZOOM Live-Cell Analysis System (Essen Bioscience) at 37°C every 2 min in the phase-contrast mode (10× objective). Tracking of live cells was done

using the manual tracking feature in Fiji (*64*). Tracks were plotted using the Chemotaxis plugin of FIJI. Cells that were in the field of imaging for fewer than two frames were discarded, as were cells which were non-adherent or floating. EL08.1D2 cells were used as de facto fiducial markers to ensure that neither they or the microscope stage was drifting and causing apparent NK cell movement. Length and displacement measurements were derived directly from tracked cells and graphed using GraphPad software. Velocity data was obtained by dividing the total track length by the time of imaging.

Zebrafish studies

Zebrafish studies were conducted in accordance with NIH guidelines for the care and use of laboratory animals and were approved by the Georgetown University Institutional Animal Care and Use Committee. Zebrafish husbandry, injections, and mounting was performed by the Georgetown-Lombardi Animal Shared Resource. Two day post fertilization stage *Tg(kdrl:mCherry-CAAX)* embryos were anesthetized with 0.016% tricaine (Sigma-Aldrich, St. Louis, MO, USA) in fish water (0.3g/L Sea Salt, Instant Ocean, Blacksburg, VA) and were injected with 100-200 NK92-GFP cells into the precardiac sinus using an air driven Picospritzer II microinjector (General Valve/Parker Hannifin) under a stereoscope. Following injection, embryos with cells in the caudal hematopoietic tissue were selected for analysis and mounted in 1.5% agarose plus 0.011% tricaine in fish water. Fish were maintained at 33°C until imaging. Confocal imaging was performed on a Leica SP8 AOBS microscope in the Georgetown-Lombardi Microscopy Shared Resource. Widefield fluorescent imaging was performed on a Keyence BZ-X inverted microscope. Images were taken at 10X across multiple z-stacks. Z-stack images were compressed using full focus and haze reduction in Keyence BZ-X software. NK

extravasation quantification was performed by counting the number of GFP cells outside red vasculature. NK extravasation quantification was performed blinded to the treatment conditions. Graphs of resulting data and statistical analysis was generated using Graphpad Prism 9.

Spheroid studies

PSC or PANC-1 spheroids were generated by plating 10,000 cells in a 0.1% agarose coated U-bottomed 96-well plate. PSC+PANC-1 spheroids were generated by plating 5,000 cells of each cell type. Aggregation was promoted by centrifuging the cells at 1000rpm for 5 minutes. Cells incubated overnight at 37°C. The next day, 1,000 NK92-GFP cells were added per well and incubated for 4 hours at 37°C. Spheroids were imaged using the Olympus IX-71 Inverted Epifluorescent Microscope at 5X. Images were analyzed in FIJI. All images underwent identical contrast enhancement and background reduction. Then a line was drawn from spheroid edge to spheroid center and GFP intensity along that line was measured. Graphs of resulting data and statistical analysis were generated in Graphpad Prism 9.

3D cluster studies

3D clusters were generated, embedded and stained as previously described (*65*, *66*). In brief, clusters were generated by plating 1,000 cells per well into 96-well Nunclon Sphera low adhesion plates (Thermo Scientific, cat#174925) and incubated overnight at 37°C. The following day, 6 clusters were embedded into an ECM containing 2,000 NK cells were plated into one well of a Nunc Lab-Tek II 8-well chamber slide (ThermoScientific, cat#154534PK). To ensure equal distribution of NK cells in Matrigel, the NK cells were first suspended in the Matrigel stock,

which was then aliquoted for individual cluster embedding. The ECM mixture consisted of 20% growth factor reduced Matrigel (Corning, 10-12 mg/ml stock concentration, #354230) and 80% rat tail collagen type I at 3mg/mL (Gibco, A1048301). Cells were either imaged for the following 24 hours every 30 minutes using a Zeiss LSM800 scanning confocal microscope enclosed in a heated chamber supplemented with CO_2 or allowed to incubate overnight at 37°C. After 24 hours, cells in matrix were fixed with 5.4% formalin for 1 hour, permeabilized with 0.5% Triton-X and blocked using goat serum. For invasion assays, NK-92-GFP cells were stained with anti-GFP (ThermoFisher, cat#A-11122). For the cell lysis assays, clusters were stained using anti-cleaved caspase 3 (Cell Signaling, cat#9661). Hoechst 33342, phalloidin, and secondary antibodies labeled with Alexa Fluor 488 nm, 546 nm, 647 nm, or 680 nm (Invitrogen) were used.

Annexin V NK cell lysis study

One day prior to assay, PSCs were stained with DiI. If donor NK cells were used, they were stained with DiO prior to the expereiment. Cells were then plated as described for the PSC-NK92 coculture assay. Following incubation period of 4 hours, all cells from a single well were collected and washed 2X with PBS. Samples were then processed by the FCSR using the Alexa Fluor 647 Annexin V and Sytox Blue staining (Biolegend). Flow data were analyzed using FloJo (v10.4.1) and statistics was performed using GraphPad Prism 9.

Supplementary Materials

Fig. S1. Human NK cells express catalytically active fibroblast activation protein.

Fig. S2. Detection of FAP on the NK cell surface.

Fig. S3. Effects of Cpd60 on cell viability.

Fig. S4. NK92-GFP cells probing for permissive sites to exit from zebrafish vasculature (red).

Fig. S5. Effects of Cpd60 on cluster area and NK cell lysis of target cells in 2D.

Movie S1: Tracking of primary NK cell migration in vehicle using phase-contrast live imaging. Images were taken 30 minutes apart for 24 hours. Each color track represents the migration path of a single NK cell.

Movie S2: Tracking of primary NK cell migration in 10 uM FAP inhibitor (Cpd60) using phase-contrast live imaging. Images were taken 30 minutes apart for 24 hours. Each color track represents the migration path of a single NK cell.

Movie S3: Time-lapse video of a NK92-GFP crawling along and extravasating from red zebrafish vasculature. Time-lapse images were taken 3 minutes apart for approximately 6 hours using confocal microscopy.

Movie S4: Time-lapse video of NK92-GFP cells migrating into PANC-1 clusters embedded in 3D matrix with vehicle. Images taken every 30 minutes for 24 hours using confocal microscopy.

Movie S5: Time-lapse video of NK92-GFP cells migrating into PANC-1 clusters embedded in 3D matrix with 10 uM FAP inhibitor (Cpd60). Images taken every 30 minutes for 24 hours using confocal microscopy.

Movie S6: Time-lapse video of NK92-GFP cells migrating into PSC clusters embedded in 3D matrix with vehicle. Images taken every 30 minutes for 24 hours using confocal microscopy.

Movie S7: Time-lapse video of NK92-GFP cells migrating into PSC clusters embedded in 3D matrix with 10 uM FAP inhibitor (Cpd60). Images taken every 30 minutes for 24 hours using confocal microscopy.

References and Notes:

1. E. Vivier, E. Tomasello, M. Baratin, T. Walzer, S. Ugolini, Functions of natural killer cells. *Nat. Immunol.* **9** (2008), pp. 503–510.

2. G. Deniz, G. Erten, U. C. Kücüksezer, D. Kocacik, C. Karagiannidis, E. Aktas, C. A. Akdis, M. Akdis, Regulatory NK Cells Suppress Antigen-Specific T Cell Responses. *J. Immunol.* **180**, 850–857 (2008).

3. T. Walzer, M. Dalod, S. H. Robbins, L. Zitvogel, E. Vivier, Natural-killer cells and dendritic cells: "L'union fait la force." *Blood*. **106** (2005), pp. 2252–2258.

4. F. D. Shi, H. B. Wang, H. Li, S. Hong, M. Taniguchi, H. Link, L. Van Kaer, H. G. Ljunggren, Natural killer cells determine the outcome of B cell-mediated autoimmunity. *Nat. Immunol.* **1**, 245–251 (2000).

5. S. Shimoda, S. Hisamoto, K. Harada, S. Iwasaka, Y. Chong, M. Nakamura, Y. Bekki, T. Yoshizumi, K. Shirabe, T. Ikegami, Y. Maehara, X.-S. He, M. E. Gershwin, K. Akashi, Natural killer cells regulate T cell immune responses in primary biliary cirrhosis. *Hepatology*. **62**, 1817–1827 (2015).

6. K. L. Belyakova, O. I. Stepanova, A. R. Sheveleva, V. A. Mikhailova, D. I. Sokolov, S. A. Sel'kov, Interaction of NK Cells, Trophoblast, and Endothelial Cells during Angiogenesis. *Bull. Exp. Biol. Med.* **167**, 169–176 (2019).

7. J. Cursons, F. Souza-Fonseca-Guimaraes, M. Foroutan, A. Anderson, F. Hollande, S. Hediyeh-Zadeh, A. Behren, N. D. Huntington, M. J. Davis, A gene signature predicting natural killer cell infiltration and improved survival in melanoma patients. *Cancer Immunol. Res.* **7**, 1162–1174 (2019).

8. B. Li, Y. Jiang, G. Li, G. A. Fisher, R. Li, Natural killer cell and stroma abundance are independently prognostic and predict gastric cancer chemotherapy benefit. *JCI Insight*. **5** (2020), doi:10.1172/jci.insight.136570.

9. H. Lee, C. Quek, I. Silva, A. Tasker, M. Batten, H. Rizos, S. Y. Lim, T. Nur Gide, P. Shang, G. H. Attrill, J. Madore, J. Edwards, M. S. Carlino, A. Guminski, R. P. M. Saw, J. F. Thompson, P. M. Ferguson, U. Palendira, A. M. Menzies, G. V. Long, R. A. Scolyer, J. S. Wilmott, Integrated molecular and immunophenotypic analysis of NK cells in anti-PD-1 treated metastatic melanoma patients. *Oncoimmunology*. **8**, e1537581 (2019).

10. E. Davis-Marcisak, A. Fitzgerald, M. Kessler, L. Danilova, E. Jaffee, N. Zaidi, L. Weiner, E. Fertig, *bioRxiv*, in press, doi:10.1101/2020.05.31.125625.

11. K. Barry, J. Hsu, M. Broz, F. Cueto, M. Binnewies, A. Combes, A natural killer-dendritic cell axis defines checkpoint therapy-responsive tumor microenvironments. *Nat. Med.* **24**, 1178–91 (2018).

12. F. Souza-Fonseca-Guimaraes, J. Cursons, N. D. Huntington, The Emergence of Natural Killer Cells as a Major Target in Cancer Immunotherapy. *Trends Immunol.* **40** (2019), doi:10.1016/j.it.2018.12.003.

13. N. Sakamoto, T. Ishikawa, S. Kokura, T. Okayama, K. Oka, M. Ideno, F. Sakai, A. Kato, M. Tanabe, T. Enoki, J. Mineno, Y. Naito, Y. Itoh, T. Yoshikawa, Phase I clinical trial of

autologous NK cell therapy using novel expansion method in patients with advanced digestive cancer. *J. Transl. Med.* **13**, 277 (2015).

14. E. Liu, D. Marin, P. Banerjee, H. A. Macapinlac, P. Thompson, R. Basar, L. Nassif Kerbauy, B. Overman, P. Thall, M. Kaplan, V. Nandivada, I. Kaur, A. Nunez Cortes, K. Cao, M. Daher, C. Hosing, E. N. Cohen, P. Kebriaei, R. Mehta, S. Neelapu, Y. Nieto, M. Wang, W. Wierda, M. Keating, R. Champlin, E. J. Shpall, K. Rezvani, Use of CAR-Transduced Natural Killer Cells in CD19-Positive Lymphoid Tumors. *N. Engl. J. Med.* **382**, 545–553 (2020).

15. J. Fayette, G. Lefebvre, M. R. Posner, J. Bauman, S. Salas, C. Even, E. Saada-Bouzid, T. Seiwert, D. Colevas, F. Calmels, R. Zerbib, A. Boyer Chammard, R. Cohen, Results of a phase II study evaluating monalizumab in combination with cetuximab in previously treated recurrent or metastatic squamous cell carcinoma of the head and neck (R/M SCCHN). *Ann. Oncol.* **29**, viii374 (2018).

16. D. Sarhan, L. Brandt, M. Felices, K. Guldevall, T. Lenvik, P. Hinderlie, J. Curtsinger, E. Warlick, S. R. Spellman, B. R. Blazar, D. J. Weisdorf, S. Cooley, D. A. Vallera, B. Onfelt, J. S. Miller, 161533 TriKE stimulates NK-cell function to overcome myeloid-derived suppressor cells in MDS. *Blood Adv.* **2**, 1459–1469 (2018).

17. M. Felices, S. Chu, B. Kodal, L. Bendzick, C. Ryan, A. J. Lenvik, K. L. M. Boylan, H. C. Wong, A. P. N. Skubitz, J. S. Miller, M. A. Geller, IL-15 super-agonist (ALT-803) enhances natural killer (NK) cell function against ovarian cancer. *Gynecol. Oncol.* **145**, 453–461 (2017).

18. E. Wennerberg, V. Kremer, R. Childs, A. Lundqvist, CXCL10-induced migration of adoptively transferred human natural killer cells toward solid tumors causes regression of tumor growth in vivo. *Cancer Immunol. Immunother.* **64**, 225–235 (2014).

19. V. Kremer, M. A. Ligtenberg, R. Zendehdel, C. Seitz, A. Duivenvoorden, E. Wennerberg, E. Colón, A.-H. Scherman-Plogell, A. Lundqvist, Genetic engineering of human NK cells to express CXCR2 improves migration to renal cell carcinoma. *J. Immunother. Cancer*. **5**, 73 (2017).

20. P. Kameritsch, J. Renkawitz, Principles of Leukocyte Migration Strategies. *Trends Cell Biol.* **30** (2020), pp. 818–832.

21. A. A. Fitzgerald, L. M. Weiner, The role of fibroblast activation protein in health and malignancy. *Cancer Metastasis Rev.* **39** (2020), pp. 783–803.

22. H. Aghajanian, T. Kimura, J. G. Rurik, A. S. Hancock, M. S. Leibowitz, L. Li, J. Scholler, J. Monslow, A. Lo, W. Han, T. Wang, K. Bedi, M. P. Morley, R. A. Linares Saldana, N. A. Bolar, K. McDaid, C. A. Assenmacher, C. L. Smith, D. Wirth, C. H. June, K. B. Margulies, R. Jain, E. Puré, S. M. Albelda, J. A. Epstein, Targeting cardiac fibrosis with engineered T cells. *Nature*. **573**, 430–433 (2019).

23. P. Busek, R. Mateu, M. Zubal, L. Kotackova, A. Sedo, Targeting fibroblast activation protein in cancer - Prospects and caveats. *Front. Biosci. (Landmark Ed.* **23**, 1933–1968 (2018).

24. J. Watt, H. M. Kocher, The desmoplastic stroma of pancreatic cancer is a barrier to immune cell infiltration. *Oncoimmunology*. **2** (2013), doi:10.4161/onci.26788.

25. M. T. Levy, G. W. McCaughan, C. A. Abbott, J. E. Park, A. M. Cunningham, E. Müller, W. J. Rettig, M. D. Gorrell, Fibroblast activation protein: A cell surface dipeptidyl peptidase and gelatinase expressed by stellate cells at the tissue remodelling interface in human cirrhosis. *Hepatology*. **29**, 1768–1778 (1999).

26. J. Barretina, G. Caponigro, N. Stransky, K. Venkatesan, A. A. Margolin, S. Kim, C. J. Wilson, J. Lehár, G. V. Kryukov, D. Sonkin, A. Reddy, M. Liu, L. Murray, M. F. Berger, J. E. Monahan, P. Morais, J. Meltzer, A. Korejwa, J. Jané-Valbuena, F. A. Mapa, J. Thibault, E. Bric-Furlong, P. Raman, A. Shipway, I. H. Engels, J. Cheng, G. K. Yu, J. Yu, P. Aspesi, M. de Silva, K. Jagtap, M. D. Jones, L. Wang, C. Hatton, E. Palescandolo, S. Gupta, S. Mahan, C. Sougnez, R. C. Onofrio, T. Liefeld, L. MacConaill, W. Winckler, M. Reich, N. Li, J. P. Mesirov, S. B. Gabriel, G. Getz, K. Ardlie, V. Chan, V. E. Myer, B. L. Weber, J. Porter, M. Warmuth, P. Finan, J. L. Harris, M. Meyerson, T. R. Golub, M. P. Morrissey, W. R. Sellers, R. Schlegel, L. A. Garraway, The Cancer Cell Line Encyclopedia enables predictive modelling of anticancer drug sensitivity. *Nature*. **483**, 603–607 (2012).

27. J. Iqbal, D. D. Weisenburger, A. Chowdhury, M. Y. Tsai, G. Srivastava, T. C. Greiner, C. Kucuk, K. Deffenbacher, J. Vose, L. Smith, W. Y. Au, S. Nakamura, M. Seto, J. Delabie, F. Berger, F. Loong, Y. H. Ko, I. Sng, X. Liu, T. P. Loughran, J. Armitage, W. C. Chan, Natural killer cell lymphoma shares strikingly similar molecular features with a group of non-hepatosplenic γδ T-cell lymphoma and is highly sensitive to a novel aurora kinase A inhibitor in vitro. *Leukemia*. **25**, 348–358 (2011).

28. S. Goda, H. Inoue, H. Umehara, M. Miyaji, Y. Nagano, N. Harakawa, H. Imai, P. Lee, J. B. Macarthy, T. Ikeo, N. Domae, Y. Shimizu, J. Iida, Matrix metalloproteinase-1 produced by human CXCL12-stimulated natural killer cells. *Am. J. Pathol.* **169**, 445–458 (2006).

29. R. P. Kitson, P. M. Appasamy, U. Nannmark, P. Albertsson, M. K. Gabauer, R. H. Goldfarb, Matrix metalloproteinases produced by rat IL-2-activated NK cells. *J. Immunol.* **160**, 4248–4253 (1998).

30. R. H. Goldfarb Nannmark, P. H. Basse, P. J. K. Kuppen, M. E. Myoung, H. Kim, R. P. Kitson, Cells and Their Inhibitors Metalloproteinases of IL-2-Activated NK Secreted and Membrane-Associated Matrix. *J Immunol Ref.* **164**, 5883–5889 (2000).

31. K. Jansen, L. Heirbaut, R. Verkerk, J. D. Cheng, J. Joossens, P. Cos, L. Maes, A.-M. Lambeir, I. De Meester, K. Augustyns, P. Van Der Veken, Extended Structure−Activity Relationship and Pharmacokinetic Investigation of (4-Quinolinoyl)glycyl-2-cyanopyrrolidine Inhibitors of Fibroblast Activation Protein (FAP). *J. Med. Chem.* **57**, 3053–3074 (2014).

32. E. M. Mace, J. T. Gunesch, A. Dixon, J. S. Orange, Human NK cell development requires CD56-mediated motility and formation of the developmental synapse. *Nat. Commun.* **7** (2016), doi:10.1038/ncomms12171.

33. B. J. Lee, E. M. Mace, Acquisition of cell migration defines NK cell differentiation from hematopoietic stem cell precursors. *Mol. Biol. Cell*. **28**, 3573–3581 (2017).

34. B. J. Lee, E. Hegewisch Solloa, M. J. Shannon, E. M. Mace, Generation of cell-derived matrices that support human NK cell migration and differentiation. *J. Leukoc. Biol.* **108**,

1369–1378 (2020).

35. H. J. Hwang, M. S. Oh, D. W. Lee, H. J. Kuh, Multiplex quantitative analysis of stroma-mediated cancer cell invasion, matrix remodeling, and drug response in a 3D co-culture model of pancreatic tumor spheroids and stellate cells. *J. Exp. Clin. Cancer Res.* **38**, 1–14 (2019).

36. M. J. Ware, V. Keshishian, J. J. Law, J. C. Ho, C. A. Favela, P. Rees, B. Smith, S. Mohammad, R. F. Hwang, K. Rajapakshe, C. Coarfa, S. Huang, D. P. Edwards, S. J. Corr, B. Godin, S. A. Curley, Generation of an in vitro 3D PDAC stroma rich spheroid model. *Biomaterials*. **108**, 129–142 (2016).

37. M. C. W. van den Berg, L. MacCarthy-Morrogh, D. Carter, J. Morris, I. Ribeiro Bravo, Y. Feng, P. Martin, Proteolytic and Opportunistic Breaching of the Basement Membrane Zone by Immune Cells during Tumor Initiation. *Cell Rep.* **27**, 2837-2846.e4 (2019).

38. A. R. M. Kurz, M. Pruenster, I. Rohwedder, M. Ramadass, K. Schäfer, U. Harrison, G. Gouveia, C. Nussbaum, R. Immler, J. R. Wiessner, A. Margraf, D. S. Lim, B. Walzog, S. Dietzel, M. Moser, C. Klein, D. Vestweber, R. Haas, S. D. Catz, M. Sperandio, MST1-dependent vesicle trafficking regulates neutrophil transmigration through the vascular basement membrane. *J. Clin. Invest.* **126**, 4125–4139 (2016).

39. M. H. Kim, R. P. Kitson, P. Albertsson, U. Nannmark, P. H. Basse, P. J. K. Kuppen, M. E. Hokland, R. H. Goldfarb, Secreted and Membrane-Associated Matrix Metalloproteinases of IL-2-Activated NK Cells and Their Inhibitors. *J. Immunol.* **164**, 5883–5889 (2000).

40. L. Zeng, S. An, E. J. Goetzl, Selective regulation of RNK-16 cell matrix metalloproteinases by the EP4 subtype of prostaglandin E2 receptor. *Biochemistry*. **35**, 7159–7164 (1996).

41. E. M. Putz, A. J. Mayfosh, K. Kos, D. S. Barkauskas, K. Nakamura, L. Town, K. J. Goodall, D. Y. Yee, I. K. H. Poon, N. Baschuk, F. Souza-Fonseca-Guimaraes, M. D. Hulett, M. J. Smyth, NK cell heparanase controls tumor invasion and immune surveillance. *J. Clin. Invest.* **127**, 2777–2788 (2017).

42. M. D. Prakash, M. A. Munoz, R. Jain, P. L. Tong, A. Koskinen, M. Regner, O. Kleifeld, B. Ho, M. Olson, S. J. Turner, P. Mrass, W. Weninger, P. I. Bird, Granzyme B promotes cytotoxic lymphocyte transmigration via basement membrane remodeling. *Immunity*. **41**, 960–972 (2014).

43. S. Iwasa, X. Jin, K. Okada, M. Mitsumata, A. Ooi, Increased expression of seprase, a membrane-type serine protease, is associated with lymph node metastasis in human colorectal cancer. *Cancer Lett.* **199**, 91–8 (2003).

44. T. Kelly, S. Kechelava, T. L. Rozypal, K. W. West, S. Korourian, Seprase, a membrane-bound protease, is overexpressed by invasive ductal carcinoma cells of human breast cancers. *Mod. Pathol.* **11**, 855–63 (1998).

45. Y. Mori, K. Kono, Y. Matsumoto, H. Fujii, T. Yamane, M. Mitsumata, W.-T. Chen, The expression of a type II transmembrane serine protease (Seprase) in human gastric carcinoma. *Oncology*. **67**, 411–9 (2004).

46. W. L. Monsky, C. Y. Lin, A. Aoyama, T. Kelly, S. K. Akiyama, S. C. Mueller, W. T.

Chen, A potential marker protease of invasiveness, seprase, is localized on invadopodia of human malignant melanoma cells. *Cancer Res.* **54**, 5702–10 (1994).

47. J. N. Arnold, L. Magiera, M. Kraman, D. T. Fearon, Tumoral immune suppression by macrophages expressing fibroblast activation protein-α and heme oxygenase-1. *Cancer Immunol. Res.* **2**, 121–6 (2014).

48. J. Tchou, P. J. Zhang, Y. Bi, C. Satija, R. Marjumdar, T. L. Stephen, A. Lo, H. Chen, C. Mies, C. H. June, J. Conejo-Garcia, E. Puré, Fibroblast activation protein expression by stromal cells and tumor-associated macrophages in human breast cancer. *Hum. Pathol.* **44**, 2549–2557 (2013).

49. G. Ghersi, Q. Zhao, M. Salamone, Y. Yeh, S. Zucker, W.-T. Chen, The protease complex consisting of dipeptidyl peptidase IV and seprase plays a role in the migration and invasion of human endothelial cells in collagenous matrices. *Cancer Res.* **66**, 4652–61 (2006).

50. P. Wäster, I. Rosdahl, B. F. Gilmore, O. Seifert, *Ultraviolet exposure of melanoma cells induces fibroblast activation protein-α in fibroblasts: Implications for melanoma invasion* (University of Crete, Faculty of Medicine, Laboratory of Clinical Virology, 2011; https://www.spandidos-publications.com/ijo/39/1/193), vol. 39.

51. A. Kennedy, H. Dong, D. Chen, W.-T. Chen, Elevation of seprase expression and promotion of an invasive phenotype by collagenous matrices in ovarian tumor cells. *Int. J. Cancer*. **124**, 27–35 (2009).

52. P. Ruan, Z. Tao, A. Tan, Low expression of miR-30a-5p induced the proliferation and invasion of oral cancer via promoting the expression of FAP. *Biosci. Rep.* **38**, BSR20171027 (2018).

53. P. C. Schuberth, C. Hagedorn, S. M. Jensen, P. Gulati, M. van den Broek, A. Mischo, A. Soltermann, A. Jüngel, O. Marroquin Belaunzaran, R. Stahel, C. Renner, U. Petrausch, Treatment of malignant pleural mesothelioma by fibroblast activation protein-specific re-directed T cells. *J. Transl. Med.* **11**, 1–11 (2013).

54. S. Kakarla, K. K. H. Chow, M. Mata, D. R. Shaffer, X. T. Song, M. F. Wu, H. Liu, L. L. Wang, D. R. Rowley, K. Pfizenmaier, S. Gottschalk, Antitumor effects of chimeric receptor engineered human T cells directed to tumor stroma. *Mol. Ther.* **21**, 1611–1620 (2013).

55. A. M. Santos, J. Jung, N. Aziz, J. L. Kissil, E. Puré, Targeting fibroblast activation protein inhibits tumor stromagenesis and growth in mice. *J. Clin. Invest.* **119**, 3613–3625 (2009).

56. E. Tran, D. Chinnasamy, Z. Yu, R. A. Morgan, C. C. R. Lee, N. P. Restifo, S. A. Rosenberg, Immune targeting of fibroblast activation protein triggers recognition of multipotent bone marrow stromal cells and cachexia. *J. Exp. Med.* **210**, 1065–1068 (2013).

57. S. Lunardi, S. Y. Lim, R. J. Muschel, T. B. Brunner, IP-10/CXCL10 attracts regulatory T cells: Implication for pancreatic cancer. *Oncoimmunology*. **4**, 1–3 (2015).

58. D. S. Aldeghaither, D. J. Zahavi, J. C. Murray, E. J. Fertig, G. T. Graham, Y.-W. Zhang, A. O'Connell, J. Ma, S. A. Jablonski, L. M. Weiner, A mechanism of resistance to

antibody-targeted immune attack. *Cancer Immunol. Res.* **7** (2019), doi:10.1158/2326-6066.CIR-18-0266.

59. S. S. Somanchi, V. V. Senyukov, C. J. Denman, D. A. Lee, Expansion, purification, and functional assessment of human peripheral blood NK cells. *J. Vis. Exp.*, 2540 (2010).

60. L. Gautier, L. Cope, B. M. Bolstad, R. A. Irizarry, affy--analysis of Affymetrix GeneChip data at the probe level. *Bioinformatics*. **20**, 307–315 (2004).

61. Z. Gu, R. Eils, M. Schlesner, Complex heatmaps reveal patterns and correlations in multidimensional genomic data. *Bioinformatics*. **32**, 2847–2849 (2016).

62. M. E. Ritchie, B. Phipson, D. Wu, Y. Hu, C. W. Law, W. Shi, G. K. Smyth, Limma powers differential expression analyses for RNA-sequencing and microarray studies. *Nucleic Acids Res.* **43**, e47 (2015).

63. H. Mi, A. Muruganujan, J. T. Casagrande, P. D. Thomas, Large-scale gene function analysis with the panther classification system. *Nat. Protoc.* **8**, 1551–1566 (2013).

64. J. Schindelin, I. Arganda-Carreras, E. Frise, V. Kaynig, M. Longair, T. Pietzsch, S. Preibisch, C. Rueden, S. Saalfeld, B. Schmid, J. Y. Tinevez, D. J. White, V. Hartenstein, K. Eliceiri, P. Tomancak, A. Cardona, Fiji: An open-source platform for biological-image analysis. *Nat. Methods*. **9** (2012), pp. 676–682.

65. Y. N. Lin, A. Nasir, S. Camacho, D. L. Berry, M. O. Schmidt, G. W. Pearson, A. T. Riegel, A. Wellstein, Monitoring cancer cell invasion and t-cell cytotoxicity in 3d culture. *J. Vis. Exp.* **2020**, 1–19 (2020).

66. J. M. Westcott, S. Camacho, A. Nasir, M. E. Huysman, R. Rahhal, T. T. Dang, A. T. Riegel, R. A. Brekken, G. W. Pearson, ΔNp63-Regulated Epithelial-to-Mesenchymal Transition State Heterogeneity Confers a Leader–Follower Relationship That Drives Collective Invasion. *Cancer Res.* **80**, 3933–3944 (2020).

Acknowledgments: We would like to thank Dr. Kerry Campbell for providing NK cell lines and continuous intellectual and technical support; Dr. Dean Lee for providing the NK feeder cells; the Georgetown Lombardi Comprehensive Cancer Center Tissue Culture and Biobanking, Flow Cytometry and Cell Sorting, Genomics and Epigenomics, and Microscopy and Imaging Shared Resources. Graphical abstract and schematics were created with BioRender.com. **Funding**: This work is supported by grants from the National Institute of Health National Cancer Institute F30 CA239441(A.A.F.), R01 CA50633 (L.M.W.), P30 CA51008 (L.M.W), and NIH-NIAID R01AI137073 to E.M.M.

Author contributions: A.A.F. and L.M.W. conceived the idea, designed the study and obtained funding. A.A.F. wrote the manuscript, conducted experiments and analyzed the data. E.F.M. and E.J.F. performed the computational analysis and E.F.M generated the computational figures. A.N. and G.P. assisted in designing and performing 3D migration experiments. E.G. assisted in conducting the zebrafish studies. S.J.J. assisted with experiment design. P.V. provided FAP inhibitor Cpd60. E.M.M. performed and analyzed the 2D migration studies and assisted with study design.

Competing interests: Elana J Fertig is on the Scientific Advisory Board of Viosera Therapeutics.

Code availability statement: The authors declare that there is no custom code in this manuscript.

Data availability statement: The public datasets analyzed in this paper are available at GEO accession GSE19067, doi: 10.1038/leu.2010.255. The authors declare that all other data supporting the findings of this study are available within the paper or its supplementary information files. All other relevant data are available from the corresponding author upon request.